Applied Catalysis B: Environmental 142–143 (2013) 633–646

Contents lists available at SciVerse ScienceDirect

Applied Catalysis B: Environmental

journal homepage: www.elsevier.com/locate/apcatb

Mechanism of degradation of ketoprofen by heterogeneous photocatalysis in aqueous solution

C. Martínez[a,b], S. Vilariño[a,b], M.I. Fernández[a], J. Faria[b], M. Canle L.[a,*], J.A. Santaballa[a]

[a] Chemical Reactivity & Photoreactivity Group, Department of Physical Chemistry & Chemical Engineering, University of A Coruña, Rúa da Fraga, 10, E-15008 A Coruña, Spain

[b] Laboratório de Catálise e Materiais, Departamento de Engenharia Química, Faculdade de Engenharia, Universidade do Porto, Rua Dr. Roberto Frias s/n, 4200-465 Porto, Portugal

ARTICLE INFO

Article history:
Received 21 January 2013
Received in revised form 8 April 2013
Accepted 9 May 2013
Available online 20 May 2013

Keywords:
Persistent organic pollutants
Pharmaceuticals
Ketoprofen
Heterogeneous photocatalysis
Advanced oxidation processes
Carbon nanotubes
Reaction mechanism
Photoproducts
Density functional theory (DFT)
SMD model

ABSTRACT

The photocatalytic degradation of ketoprofen (**KP**), 2-(3-benzoylphenyl)-propionic acid, was studied under UV–vis irradiation using synthesized TiO_2 (anatase), composites of multi-walled carbon nanotubes with TiO_2 anatase (20-MWCNT–TiO_2), and commercial anatase. Different factors that affect this process are compared: irradiation source, load of catalyst, initial concentration of **KP**, pH, concentration of dissolved oxygen, addition of co-oxidants, and the presence of *tert*-butanol as $HO^{\bullet}$ scavenger. The fastest degradation of **KP**, with a rate constant $(42 \pm 3) \times 10^{-4}\ s^{-1}$, was obtained under UV irradiation in air atmosphere, using $1.2\ g\,L^{-1}$ of 20-MWCNT–TiO_2. Composites of 20-MWCNT–TiO_2 also afforded the fastest degradation with UVA–vis irradiation, in the absence of oxygen, with a rate constant $(13.6 \pm 0.7) \times 10^{-4}\ s^{-1}$. In this case, 60% mineralization of **KP** was observed after 30 min. Gibbs free energies, pK_a values, and the standard reduction potential of **KP** and related species, calculated by DFT (6-311G(d,p)), are in agreement with the observed behavior.

A feasible degradation mechanism is proposed, both for the photolysis and photocatalyzed processes. Similar transient species are involved, both routes leading to similar photoproducts, the main is (3-ethylphenyl)(phenyl)methanone (m/z = 211 g/mol), resulting from decarboxylation of **KP**.

1. Introduction

Pharmaceuticals and personal care products (PPCP) constitute a wide and extraordinarily varied group of organic compounds. Due to their continuous input into the environment, they behave as persistent organic micropollutants, ubiquitously found in the aquatic environment, including sewage, surface, ground, and drinking water [1].

A large number of publications have reported in the last few years environmental concentrations of PPCPs in the range of ppb in different environmental compartments [2]. Some ecotoxicological studies showed the chronic toxicity of different PPCPs toward aquatic organisms due to continuous exposure to low doses [3]. Thus, there is a need for additional studies on the effects and possible interactions of different PPCPs [4]. Their low volatility leads to the distribution of PPCPs in the environment taking place mainly through aqueous transport and food-chain dispersion. Their polar – non volatile nature avoids them escaping from aquatic systems [5].

Spain is one of the World's largest consumers of pharmaceuticals [3]. Recent studies on the presence of ketoprofen (**KP**) showed this pharmaceutical occurred in more than 80% of the samples in the Henares–Jarama–Tajo river system (Madrid, Spain) [6], and in the 100% of the influent and effluent samples from urban wastewater treatment plants located in the area of Castelló (Valencia, Spain) [7].

Ketoprofen, (RS)2-(3-benzoylphenyl)-propionic acid (Scheme 1) is a non-steroidal anti-inflammatory drug (NSAIDs), widely used for the treatment of rheumatoid arthritis, osteoarthritis, ankylosing spondylitis, and also for non-rheumatoid diseases or postoperative pain. This pharmaceutical contains benzophenone as chromophore, and undergoes photosensitization giving rise to undesired photoallergic effects on human skin, like hypersensitivity and *myasthenia gravis* [8–10]. Such effect is a consequence of a specific immune reaction, **KP** forming an immunogenic complex that causes the allergic reaction [11]. On the other hand, **KP** has been recently used in the development of phototriggers and ketoprofenate photocages [12].

The behavior of ketoprofen under irradiation in solution has been extensively analyzed, both from the analytical and kinetic point of view. Its mechanism of photodegradation has been studied by fast transient absorption measurements [13–16] and

* Corresponding author. Tel.: +34 981167000; fax: +34 981167065.
E-mail address: mcanle@udc.es (M.C. L.).

0926-3373/$ – see front matter © 2013 Elsevier B.V. All rights reserved.
http://dx.doi.org/10.1016/j.apcatb.2013.05.018

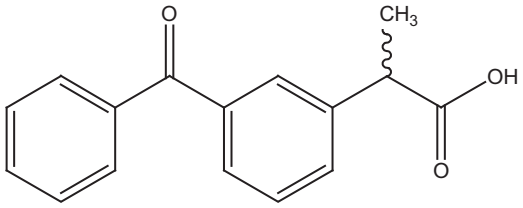

KP

Scheme 1. Chemical structure of Ketoprofen (KP).

time-resolved laser-induced optoacoustic calorimetry [17]. In addition quantum chemical calculations [8,18], and product analysis [19,20], have been used to complete the picture.

KP shows rather uncommon chemistry for a substituted benzophenone. Due to the presence of the carboxylic group (aqueous pK_a *ca.* 4.7) [13,15], **KP** may occur as the neutral form or as the anion **KP**$^-$, depending on the pH of the medium (Schemes 2–5). Upon irradiation with $\lambda > 300$ nm neutral **KP** behaves as a conventional benzophenone due to the high efficiency of intersystem crossing (ISC) to form an excited triplet (^{3}**KP**), while **KP**$^-$ decarboxylates.

As shown in Scheme 5 the monophotonic excitation of ketoprofen carboxylate (**KP**$^-$) produces mainly the triplet (^{3}**KP**$^-$), which undergoes a rapid and efficient photodecarboxylation reaction ($\varphi = 0.75$ at pH *ca.* 7.4) [20], yielding a carbanion (**CA**$^-$), that is structurally resonant with 3-ethylbenzophenone ketyl biradical anion (^{3}**BC**$^-$), for which a lifetime *ca.* 200 ns was reported in water [21]. This species could then protonate (k_{H^+/H_2O} *ca.* 3×10^7 s^{-1}) [21] to produce either 3-ethylbenzophenone (**1**) or the 3-ethylbenzophenone ketyl biradical (^{3}***BCH***) that, after ISC and intramolecular hydrogen transfer, yields the main final photoproduct **1** (Schemes 2–5) [19,22].

Upon photoexcitacion **KP**$^-$ could also absorb another photon to generate in minor extent (<10%) the corresponding neutral radical (**KP**$^\bullet$) that rapidly decarboxylates to **BC**$^\bullet$ ($k > 1 \times 10^7$ s^{-1}) [13,14], which leads to different photoproducts (**2**, **3**, **4**, **7**, **11**, **12**) depending on the experimental conditions (Scheme 2) [22–25].

The degradation of **KP** in aqueous solution was studied by pulse and γ-radiolysis. The final result of the reactions of HO$^\bullet$ with **KP** (*k ca.* 6×10^9 mol^{-1} dm^3 s^{-1}) [26] leading to hydroxycyclohexadienyl type radical intermediates is the formation of several hydroxylated **KP** derivatives (**12**) [27]. The hydrated electron formed in these experiments reduces the carbonyl oxygen (*k ca.* 2×10^{10} mol^{-1} dm^3 s^{-1}), that rapidly protonates to give **KP** ketyl radical (**KPH**$^\bullet$) [28]. This behavior is well documented for benzophenone [29,30].

TD-DFT calculations of the **KP** excited state potential energy surfaces predict **KP**$^-$ decarboxylation through the triplet state, which shows a small barrier from low-lying excited singlets, whereas the neutral form **KP** would not decarboxylate easily [8].

Electronic structure calculations, at the CASSCF/CASPT2 level suggested that under 330 nm irradiation the decarboxylation of the anion is initiated by a long-distance charge transfer excited state, while for the neutral form and at $\lambda < 260$ nm involves a short-distance charge transfer excited state upon photoexcitation [31].

Phillips et al. have found that irradiation of aqueous acid solution under 266 nm causes the decarboxylation of neutral **KP** through excited-state intramolecular proton transfer (ESIPT) leading to the biradical intermediate ^{3}**BCH**. Loss of CO_2 takes place slowly compared to **KP** carboxylate [32].

These results support the hypothesis of the special photochemical behavior of **KP** toward the photolytic degradation as coming from its low lying triplet excited state [8,15–17]. The detailed reaction mechanism for the photolytic degradation has been described using both time-resolved resonance Raman spectroscopy and quantum chemical calculations [33,34].

Advanced oxidation processes (AOPs) [35,36], can be broadly defined as aqueous phase oxidation methods based on the intermediacy of highly reactive and scarcely selective radical species such as HO$^\bullet$, $O_2^{\bullet -}$, $HO_2^\bullet$, and other reactive oxygen species (ROS). Heterogeneous photocatalysis is one of the most commonly used AOPs, leading in many cases to complete mineralization of the pollutant, independently of its organic or inorganic nature [36].

TiO_2 is largely used in heterogeneous photocatalysis to degrade a wide range of pollutants due to its wide band gap (3.03 eV for rutile, 3.18 eV for anatase) [37]. It shows many advantages such as: easy operation under common environmental conditions [36], inexpensive, commercially available in various crystalline forms and particle characteristics, low toxicity and photochemical stability [36,38–41]. Its major drawback is its low spectral overlap with sunlight emission, only about 5%.

Here, we report the mechanism of photocatalytic degradation of aqueous **KP** using synthesized nanocrystalline TiO_2 (anatase), 20-multi-walled carbon nanotubes, 20:100 MWCNT–TiO_2 (w:w) composites, as well as the commercial form P25 as photocatalysts. We have studied the effects of source of irradiation, initial **KP** concentration, type and load of photocatalyst, partial pressure of oxygen, pH, addition of H_2O_2 and t-BuOH (HO$^\bullet$-scavenger).

2. Experimental

KP VETRANAL®, analytical standard, was purchased from Sigma–Aldrich and used without further purification. Tert-butanol, 99.5% purity, from Janssen Chimica, was used without further purification. Commercial TiO_2 anatase powder, 99.8% purity based on trace metal analysis, was from Sigma-Aldrich. MWCNT, 95% purity, main range of diameter = 10–20 nm; length = 5–15 μm, synthesized by catalytic decomposition of CH_4, from Shenzhen Nanoport Co. Ltd., China, was used as received.

Milli-Q Direct water was obtained from a Millipore apparatus with a resistivity of 18.2 MΩ cm at 298 K and a total organic carbon load of less than 5 μg L^{-1}. Triply distilled water was also used for washing purposes. O_2 and Ar used were ALPHAGAZ™ 1 brand by Air Liquide, with a maximum impurity level (ppm vol) of $H_2O < 3$ and $C_nH_m < 0.5$. Ar showed also a maximum impurity level of $O_2 < 2$ ppm vol. Both gases are N50 compliant, which guarantees a minimum purity of 99.999% (mol). Unless otherwise indicated, experiments were carried out at the natural pH corresponding to dissolved **KP** ($pH_{nat,KP} \approx 4.5$), at which approximately half **KP** molecules are deprotonated (pK_a (**KP**$^-$/**KP**) = 4.45) [42].

TiO_2-based photocatalyst have different zero-charge points: $pH_{PZC} = 6.30$ for P25 and 6.0 ± 0.9 for anatase [43]. Hence, the surface of the photocatalyst was protonated at the working pH. The pH of the solution changed up to *ca.* 5.8 when TiO_2 was added, and did not undergo significant variations through the experiments. No buffers were used to avoid the interference of nucleophiles and/or electrophiles.

2.1. Photocatalysts

Nanocrystalline TiO_2 catalysts were obtained using an acid-catalyzed sol–gel method [44] starting from titanium isopropoxide at room temperature. $Ti(OC_3H_7)_4$ (Aldrich 97%) was dissolved in acidified EtOH (Panreac PA), the solution stirred magnetically for 30 min, and then a small amount of HNO_3 (Fluka 65%) added. The alkoxide undergoes hydrolysis, and then condensation between two ≡Ti—OH or between ≡Ti—OH and ≡Ti—OC_3H_7 takes place, yielding ≡Ti—O—Ti≡. Acid catalyzed hydrolysis controls the rate of this step avoiding TiO_2 precipitation. The mixture was loosely

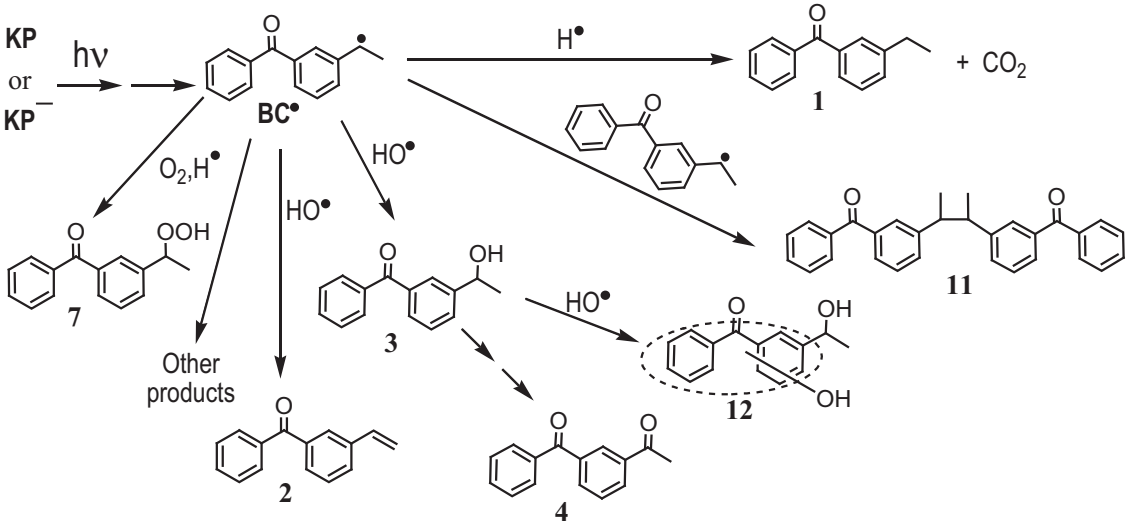

Scheme 2. Photoproducts found in **KP** direct photolysis in aqueous solution.

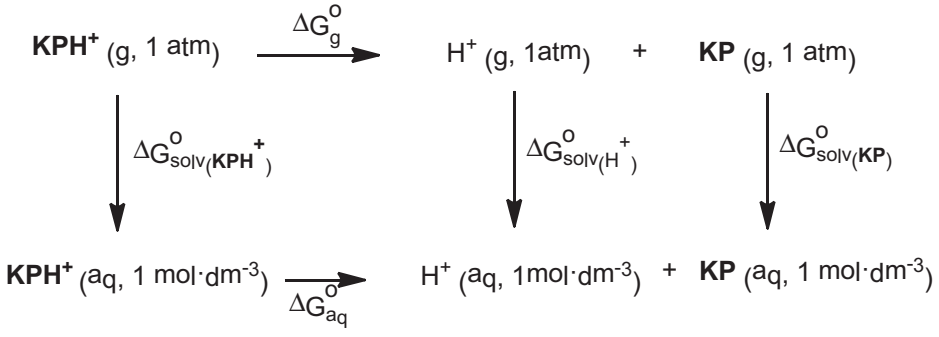

Scheme 3. Thermodynamical cycle used for calculation of pK_a values.

covered and kept stirring until a homogenous gel formed, which was aged in air for several days. Then, the xerogel was crushed into a fine powder and dried at room temperature. The powder was calcined at 673 K under N_2 flow for 2 h to obtain anatase-TiO_2.

The MWCNT–TiO_2 composite catalyst was produced using a MWCNT to TiO_2 weight ratio 1:20, *ca.* 17% MWCNT in the photocatalyst. The procedure was similar to the described before, the MWCNT being introduced into the $Ti(OC_3H_7)_4$ ethanolic solution. The obtained powder was also calcined at 673 K under N_2 flow for 2 h. Hereafter, the so-formed composite will be referred to as 20-MWNT-TiO_2 [45]. TiO_2 P25, in what follows labeled as P25, was used for comparison purposes.

Wang et al. [45] found that the BET surface was, for the synthesized anatase and 20-MWCNT–TiO_2, respectively, 107

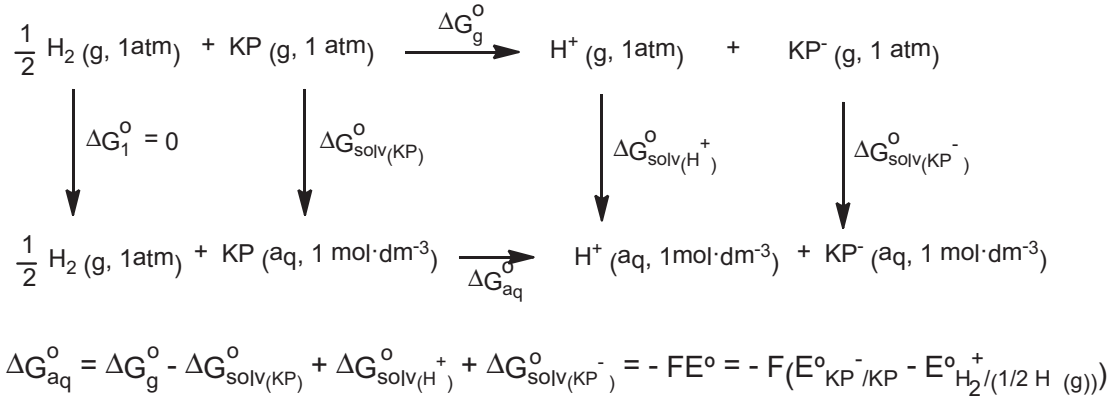

Scheme 4. Thermodynamical cycle used in the calculation of theoretical reduction electrode potential.

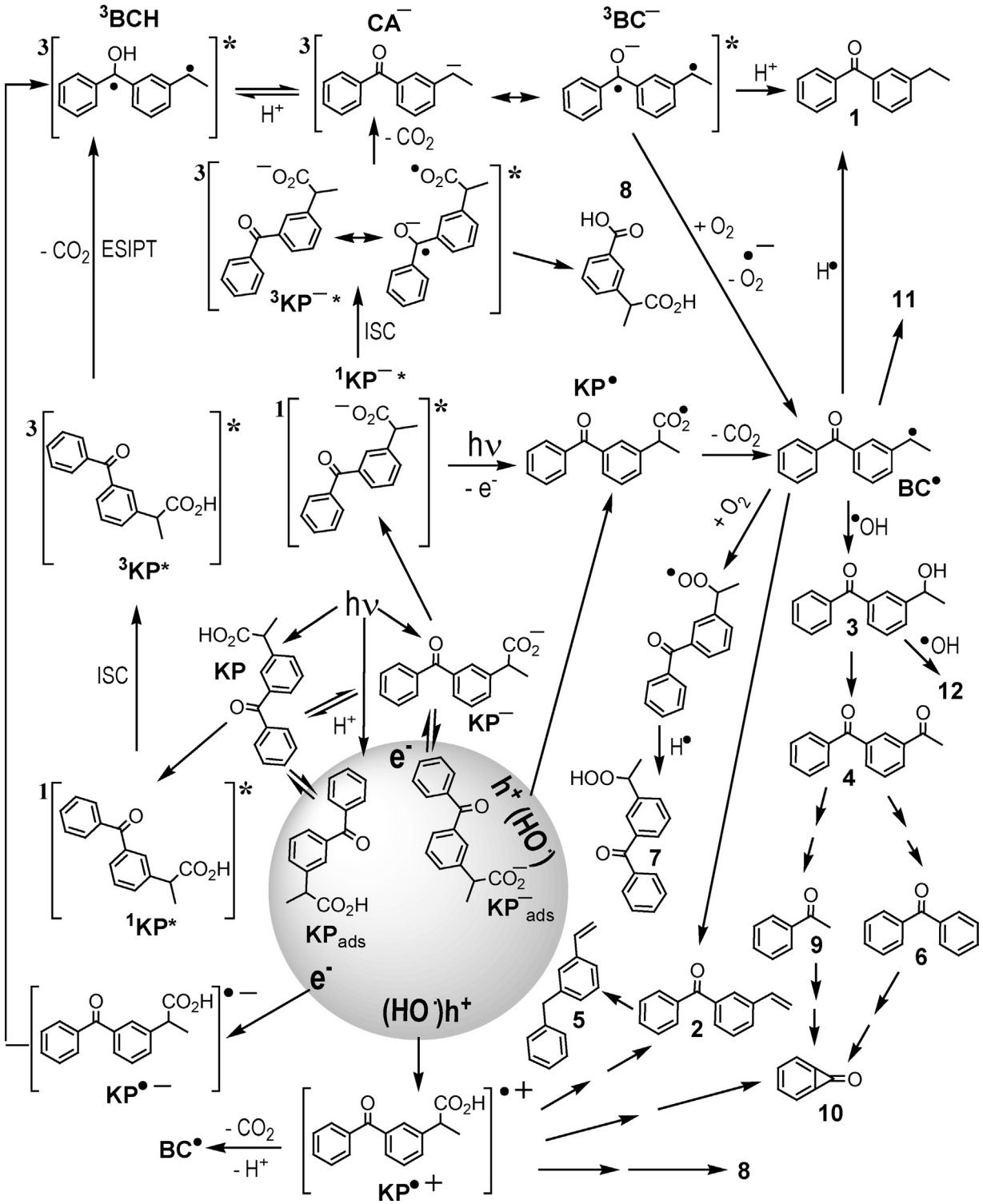

Scheme 5. Reaction mechanism for the photodegradation, photolytic and photocatalytic, of ketoprofen in aqueous solution.

and 139 m^2/g, while the pore size diameters were *ca.* 3.2 and 3.5 nm. The average pore size distribution and TiO_2 crystal size (d_{TiO_2}) for synthesized anatase and 20-MWCNT–TiO_2 were 8.5 ± 0.2 nm and 7.4 ± 0.1 nm, respectively. The BET surface of commercial anatase is 38 m^2/g [41]. Diffuse reflectance UV–vis spectra of these catalysts have already been reported [45,46].

2.2. Photocatalytic degradation experiments

The photocatalytic degradation of **KP** was carried out at room temperature (*ca.* 293 K) in aqueous solution upon UV–vis irradiation. The experiments were carried out in a 1000 mL glass immersion photochemical reactor (Ø = 8.5 cm) charged with 800 mL of solution or suspension, and the irradiation lamp, located

axially in the reactor inside a quartz immersion tube. The reactor was equipped with:

(a) A Heraeus TQ 150 medium-pressure Hg-vapor lamp, for which the more intense emission lines occur at λ_{exc} = 254, 313, 366, 405, 436, 546 and 578 nm. The UV emission lines at λ_{exc} < 366 nm were filtered out using a DURAN 50® glass jacket, filled with water. The photon flux at 366 nm was 2.38×10^{-6} Einstein s^{-1} as determined by potassium ferrioxalate ($K_3[Fe(C_2O_4)_3]$) actinometry [47].
(b) A Heraeus TNN 15/32 low-pressure Hg-vapor lamp, which λ_{exc} = 254 nm, 3 W radiant flux. The photon flux at 254 nm was 3.33×10^{-8} Einstein s^{-1}, determined by $K_3[Fe(C_2O_4)_3]$ actinometry [47].

In both cases, a circulating water jacket was used to keep the temperature of suspensions within 293 ± 1 K.

In a typical experiment the initial concentration (C_0') of the substrate was set at 59 μM. The fact that this concentration is higher than typical environmental values would not induce any change in the reaction mechanism, or in the reaction products [48].

The amount of suspended TiO_2 was kept at 1 g L^{-1}. In the case of TiO_2 and MWCNT catalysts, the amount of solid was calculated by keeping the same amount of TiO_2. A 200 mL min^{-1} O_2/Ar (50 vol.% of oxygen) stream was continuously bubbled through the solution. A dark experiment was carried out for each catalyst during 60 min, checking that the adsorption–desorption equilibrium was established within 30 min, without significant spectral changes after this time. Before inserting the lamp in the reaction medium, previously ignited and warmed up, the suspensions were gas-saturated and magnetically stirred for 30 min. The first sample was taken at the end of the dark adsorption period, just before the lamp was inserted, in order to determine the concentration of the compound in solution, which was taken as C_0 for each experiment. Then, the suspensions were irradiated with UV or UVA–vis light at constant stirring speed. Reactions were stopped after 3–5 h of irradiation. Aliquots were withdrawn from the reactor at different reaction times and centrifuged for 10 min at 14,500 rpm immediately prior to analysis.

Langmuir–Hinshelwood model (Eq. (1)) was used to analyze photocatalysis kinetic curves:

$$r = k_{LH} \times \Theta = k_{LH} \times \frac{K_{LH} \times C}{1 + K_{LH} \times C} \quad (1)$$

where k_{LH} (mol s^{-1} cm^{-2}) is an apparent kinetic rate constant per unit of surface area, Θ (cm^2) accounts for the coverage of the catalyst surface by the substrate, K_{LH} is the Langmuir–Hinshelwood adsorption constant, and C is the concentration of the substrate in bulk solution once the equilibrium has been established.

2.3. Analytical methods

Once the samples were centrifuged, the clean transparent solutions were analyzed by different techniques:

(a) UV–vis spectroscopy, performed in a JASCO V-560 UV–vis spectrophotometer equipped with a double monochromator and double beam optical system (200–600 nm).
(b) Analyses were made using a Thermo Accela HPLC equipped with a PDA detector, coupled to a Thermo LTQ Orbitrap Discovery mass spectrometer using ESI^+/ESI^- ionization, operating in full-scan mode (R > 30,000), between 100 and 400 uma. Separation was carried out using a Phenomenex Luna C18 column (150 mm × 4.6 mm × 5 μm) at a flow rate of 0.5 μL min^{-1}. Mobile phases were water 3.3 mM formic acid (A) and methanol (B), and the gradient was as follows: 0 min, 70% A; 1 min, 70% A; 5 min, 10% A; 15 min, 10% A; 17 min, 70% A; 21 min, 70% A.
(c) Total organic carbon (TOC) measurements were performed in a Shimadzu TOC-5000 analyzer equipped with a non-dispersive infrared gas detector (NDIR) and ASI 5000A Shimadzu autosampler. The combustion tube was filled with platinum catalyst (Shimadzu) for determination of total carbon (kept at 953 K). High purity synthetic air, at a flow of 150 mL min^{-1}, and ultrapure Millipore water (Milli-RX 20, MilliQ 185) were used. The standard used for determination of total carbon was potassium acid phtalate *p.a.* ($KHC_8H_4O_4$, Shimadzu), Na_2CO_3 *p.a.* and $NaHCO_3$ *p.a.* for inorganic carbon.

2.4. Theoretical calculations

All computations in this work were carried out using the Gaussian09 suite of programs [49] and the B3LYP/6-311++G(d,p) methodology. The triple-ζ basis set 6-311++G(d,p) includes one set of diffuse functions and another set of polarizations functions for all atoms. All geometries included in this work correspond to energy minima, checked through analytical vibrational frequencies. Redox potentials and pK_a values were computed following Schemes 3 and 4.

The standard Gibbs free energy for the formation of H^+(g) (−6.28 kcal mol^{-1}), was calculated by using the Sackur–Tetrode equation, which reduces to −4.39 kcal mol^{-1} when the change of reference state, from atm to mol L^{-1}, is considered. The value for the solvation free energy of H^+, has been taken as–264 kcal mol^{-1} [50]. It is worth remarking that the precision of the calculated pK_a values partly relies on the accuracy of this value. The solvation free energy for water was taken as −6.32 kcal mol^{-1} [50].

Solvation free energies were calculated with the continuum solvation model SMD [51] as implemented in Gaussian09 [49].

3. Results and discussion

3.1. Ketoprofen adsorption onto the photocatalysts

The extent of **KP** adsorption on synthesized anatase during the dark phase (absorbance at t = 0 and 30 min) is *ca.* 10%. Thus, assuming the adsorption–desorption equilibrium is established effectively, the variations of the adsorption properties are negligible when the solution is irradiated, the surface of the catalyst is homogeneous, the different active adsorption sites are equivalent, and a single layer of **KP** is formed onto the surface of the catalyst. The Langmuir adsorption equilibrium constant can be estimated as K_L = 7.5 M^{-1} for the adsorption of **KP** onto the synthesized anatase in aqueous solution. 81% adsorption extent is observed for experiments with 1.2 g L^{-1} of 20-MWCNT–TiO_2 (*i.e.*, 1.0 g L^{-1} TiO_2) under the same assumptions.

3.2. Photocatalytic degradation of ketoprofen

The rate and efficiency of photocatalytic reactions depends on a number of variables: irradiation energy, initial concentration of compound, type and load of catalyst, pH, oxygen concentration, and the addition of co-oxidants or scavengers. Here, we describe the effect of all these variables.

Fig. 1 shows the UV–vis absorbance spectra and the time-resolved absorption spectra for the photolytic degradation of **KP** upon irradiation at 254 nm. The extinction coefficient for **KP** at the maximum absorbance wavelength (259 nm) and *natural* pH (*ca.* 5) of the solution is ϵ = 15,469 mol^{-1} dm^3 cm^{-1}.

KP undergoes photodegradation under UV aqueous irradiation in a pure photolytic regime. The presence of three deformed

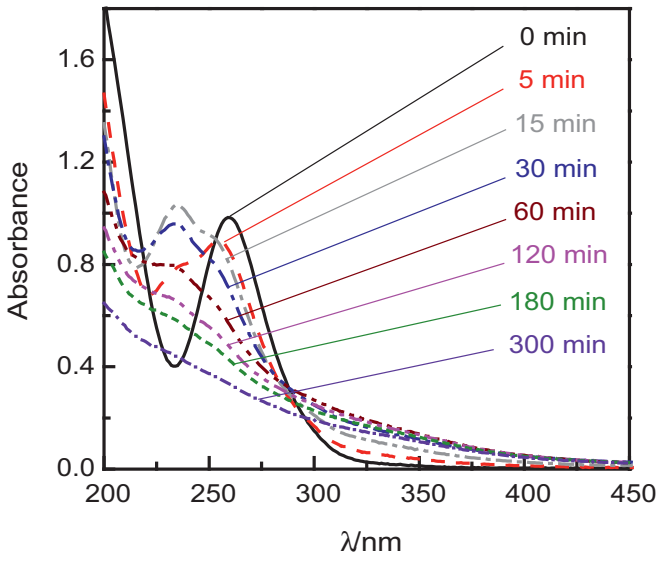

Fig. 1. Time-resolved UV–vis spectra following aqueous irradiation of **KP** at 254 nm. [KP] = 59 μM, pH = 4.5, P(O_2) = 21% (v/v); *T ca.* 293 K. Spectra recorded at the indicated times.

isosbestic points suggests the concurrence of, at least, two photodegradation processes, the second becoming evident only after *ca.* 15 min. One of the photoproducts peaks at 234 nm, within the first 5 min, and disappears after *ca.* 20 min. Similarly, another product absorbing at *ca.* 250 nm forms and then fades.

KP also undergoes aqueous degradation in the presence of photocatalysts, both under UV and UVA–vis irradiation (Fig. 2). Analysis of **KP** by HPLC/MS/MS showed that its complete removal takes approximately 15 min in different conditions: UV irradiation under air or in anaerobic conditions and 3 mM hydrogen peroxide, and UVA–vis irradiation in anaerobic conditions, always with 1 g L^{-1} of anatase.

Both photocatalyzed and direct photolysis of **KP** follow pseudo-first order decay kinetics (Table 1). Assuming the reaction occurs between species that are adsorbed onto the solid surface of the catalyst and that the reaction of **KP** with HO• and/or h^+

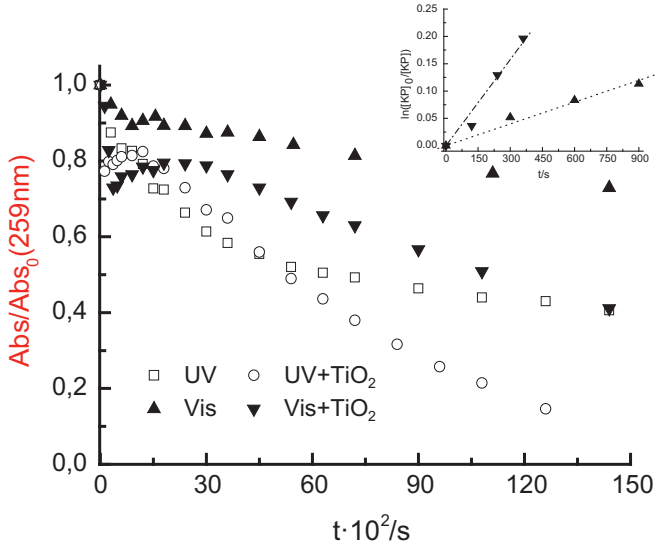

Fig. 2. Degradation of aqueous **KP** upon irradiation with a low-pressure Hg lamp and a medium-pressure Hg lamp in the presence and absence of a photocatalyst. [anatase] = 1.0 g L^{-1}; pH ≈ 4.6; $[KP]_0$ = 59 μM; P(O_2) = 21% (v/v); *T ca.* 293 K. Inset: estimation of k_{app}.

(reactive species) is much lower than the disappearance of the reactive species [52], the photodegradation of **KP** aqueous solution by UVA–vis irradiation would follow pseudo-first-order kinetics with respect to the organic compound concentration according to the Langmuir–Hinshelwood model (Eq. (1)) [53]. Under the assumptions used in this work the Langmuir–Hinshelwood adsorption (KLH) should coincide with the Langmuir adsorption constant (see Section 3.1).

From our data, K_{LH} has been roughly calculated as K_{LH} 7540 M^{-1} for synthesized anatase. If the concentration of **KP** is low enough, *i.e.* $K_{LH} \cdot C < 1$, Eq. (1) reduces to the typical first order kinetic equation (Eq. (2)). Therefore, $k_{obs} = k_{app}$.

$$r = \frac{dC}{dt} = (k_{photolysis} + k_{photocatalysis}) \cdot C = k_{app} \cdot C \quad (2)$$

where k_{app} depends on the initial concentration of **KP**.

Integration, with the restriction $C = C_0$ when $t = 0$, leads to a linear plot of $\ln(C/C_0)$ *vs. t*:

$$\ln\frac{C_0}{C} = k_{app} \cdot t + \text{constant} \quad (3)$$

A number of experiments were carried out by continuous monitorization of absorbance *vs.* time. Due to spectral overlapping between **KP** and the obtained photoproducts (Fig. 1), the rate constants (k_{app}) were calculated using the absorbance values at the initial stages of the process [54]. The following figures of the manuscript show the time resolved spectra at 259 nm, absorbing wavelength of KP. The corresponding rate constants and half-life times for **KP** disappearance are compiled in Table 1. When discontinuous HPLC monitorization was used, a good agreement was found between rate constants obtained by both methods, k_{app} (UV–vis) = $(13.6 \pm 0.7) \times 10^{-4}$ s^{-1} *vs.* k_{app} (HPLC) = $(17 \pm 2) \times 10^{-4}$ s^{-1}.

As expected, the UV-initiated process, with or without catalyst, is faster than with UVA–vis light. The pure photocatalytic process competes with the photolytic process; the contribution of the former to the UV and UVA–vis irradiation photodegradation rate constant is *ca.*, respectively, 15% and 25%. The photodegradation rate increases when a photocatalyst is used, the fastest process being observed with 20-MWCNT–TiO_2, for which the rate contant is approximately twice as that for anatase with both types of irradiation sources.

Light scattering by the suspended catalyst nanoparticles inside the photoreactor is one of the main factors of reduction of both the photodegradation quantum yield ($\Phi_{photodegradation}$) and the photonic efficiency of the process (ξ) [55]. A metal oxide such as TiO_2 does not absorb all the incident photon flow [55]. Another important factor of reduction of $\Phi_{photodegradation}$ and ξ could be the surface characteristics of the photocatalyst involved in the process, directly related to the method of synthesis of the catalyst. Thus, the results obtained in identical conditions with TiO_2 that has been synthesized by different methods may be dissimilar [56].

In a pure photolytic regime photolysis quantum yield ($\Phi_{Photolysis}$) could be defined as the ratio of moles of compound transformed to Einstein absorbed. Similarly, in a pure photocatalytic regime, the photocatalysis quantum yield ($\Phi_{Photocatalysis}$) would be the ratio of moles of reactant consumed, or product formed, in the bulk phase per Einstein absorbed by the photocatalyst [57]. In both cases, the photodegradation quantum yield could be calculated using the following equation [58–60]:

$$\Phi_{photodegradation} = \frac{k_{app}}{2.303 \times I_\lambda \times \varepsilon_\lambda \times l} \quad (4)$$

where $\Phi_{photodegradation}$ is the photodegradation quantum yield, k_{app} (s^{-1}) is the apparent pseudo first order rate constant, I_λ (Einstein L^{-1} s^{-1}) is the light intensity at wavelength λ, ϵ_λ

Table 1
Apparent rate constants (k_{app}), half-life times, photodegradation quantum yields ($\Phi_{photodegradation}$), photonic efficiency (ξ), and electrical energy efficiency (E_{EO}) for the photolytic and photocatalytic aqueous degradation of **KP**. $[KP]_0 = 59\ \mu M$, [anatase] = 1.0 g L^{-1}, [20-MWCNT–TiO_2] = 1.2 g L^{-1} (*i.e.*, 1.0 g L^{-1} of TiO_2), $P(O_2) = 21\%$ (v/v), pH *ca.* 5, *T ca.* 293 K.

Lamp	Catalyst	$k_{app} \times 10^4/s^{-1}$	$t_{1/2} \times 10^{-3}/s$	Φ (%)	ξ (%)	E_{EO}/kW L^{-1} s^{-1}
UV (254 nm)	None	3.3 ± 0.4	2.1	0.24	0.15	2182
	Anatase	21.5 ± 0.6	0.3	1.56	0.95	335
	20-MWCNT–TiO_2	42 ± 3	0.16	3.05	1.86	171
UVA–vis (366 nm)	None	1.33 ± 0.07	5.2	0.04	0.0008	54,135
	Anatase	5.3 ± 0.4	1.3	0.17	0.0033	13,585
	20-MWCNT–TiO_2	9.0 ± 0.6	0.77	0.29	0.0056	8000

(cm^{-1} mol dm^{-3}) is the molar absorptivity at wavelength λ, and l is the cell path length (cm). The obtained photodegradation quantum yields ($\Phi_{photodegradation}$) are shown in Table 1.

The photonic efficiency (ξ) can be defined as the ratio of moles of reactant molecules transformed, or product molecules formed, to Einstein of incident photons absorbed by the reactor [61]. This parameter is also known as initial apparent quantum yield (Φ_{app}). For a primary photochemical process (an elementary process), $\xi = \Phi$ [62].

The photonic efficiency (ξ) can be determined by the ratio of the initial reaction rate (k'_{app}) to the efficient photonic flux in Einstein per second (φ), Eq. (5).

$$\Phi_{photodegradation} = \frac{k_{app}}{2.303 \times I_\lambda \times \varepsilon_\lambda \times l} \quad (5)$$

Its maximum theoretical value is unity, but considering the nature of the catalyst, the experimental conditions and, specially, the type of the reaction considered, the obtained values may be rather variable [63]. The values obtained for the photonic efficiency (ξ) are compiled in Table 1. From the obtained values, ξ is much better for the photocatalytic process as compared to the photolytic process. Also, ξ is better for UV, as compared to UVA–vis. The value $\xi = 1.86$, obtained when using 20-MWCNT–TiO_2 with UV, points to the existence of additional processes, related to the intrinsic nature of the composite that improve the efficiency of the incident photons. A working hypothesis may be that while UVA–vis has enough energy to overcome the energy gap between valence and conduction bands in TiO_2, this may not the case for MWCNT. The much more energetic UV light may have enough energy to induce the equivalent electronic transition in MWCNT, that can be semiconductors depending on their helicity [64]. In this way the photocatalytic process could feed back, increasing ξ.

Among the factors taken into account in selecting a method for the degradation of pollutants, one of the most important is economy. Photodegradation of organic micropollutants in aqueous solution is an energy demanding process, electric energy being the major factor of operating cost. The electrical energy efficiency (E_{EO}) is defined as the number of kWh of electrical energy required to reduce the pollutant concentration by one order of magnitude in 1 m^3 of contaminated water. E_{EO} (kW L^{-1} s^{-1}) can be calculated according to Eq. (6) [65,66]:

$$E_{EO} = \frac{P \times t \times 1000}{V \times 60 \times \log(C_0 \times C_f)} \quad (6)$$

where P is the electric power consumed by the lamp (kW), t is the irradiation time (s), V is the volume (L) of the solution in the reactor, C_0 and C_f are the initial and final concentrations of the organic micropollutant. Taking into account Eqs. (3) and (6), E_{EO} could be expressed as:

$$E_{EO} = \frac{38.4 \times P}{V \times k_{app}} \quad (7)$$

E_{EO} is independent of the type and intensity of irradiation, flow rate, and reactor volume [67]. The values obtained for the electrical energy efficiency (E_{EO}) are collected in Table 1. It is worth to remark that the electrical efficiency is better for the photocatalytic process as compared to the photolytic process, and that E_{EO} is, by far favorable to UV rather than UVA–vis.

MWCNT/TiO_2 mixtures can be very efficient as photocatalysts [68,69]. Two mechanisms explain such synergistic effect: (i) following light absorption ($h\nu \geq E_G$) an e^- is promoted from the valence band (VB) to the conduction band (CB) of TiO_2, and subsequently transferred into MWCNTs, leaving positive holes (h^+) on TiO_2, available to act as oxidants [70,71]. (ii) MWCNTs transfer e^- to the CB of TiO_2, with reduction of surface-adsorbed O_2 to $O_2^{\bullet -}$, while e^- are removed from the VB by positive charges in MWCNTs, leaving h^+, available to act as oxidants. Upon migration to the surface, h^+ on TiO_2 can react with adsorbed H_2O to form $HO^\bullet$ [45,70].

In addition, C—O—Ti bonds in MWCNT–TiO_2 extend light absorption to longer wavelengths, improving the photoefficiency of the process, and the resulting electronic configuration increases the photoactivity, as compared to similar composites [70,72].

3.2.1. *Effect of the initial concentration of **KP***

The initial **KP** concentration was varied from 4.8 to 59 μM. The results showed that upon 366 nm irradiation, the reaction rate decreases as the initial concentration of aqueous **KP** increases (Fig. 3 and Table 2).

The observed rate constant for the reaction with 4.8 μM **KP** was $k_{app} = (9.6 \pm 0.5) \times 10^{-4}\ s^{-1}$ which reduced by *ca.* 45% to $k_{app} = (5.3 \pm 0.4) \times 10^{-4}\ s^{-1}$ in the presence of 59 μM **KP**. Thus, a reduction of [**KP**] by one order of magnitude duplicates the reaction rate. Intuitively, as $[\mathbf{KP}]_0$ increases the probability of reaction

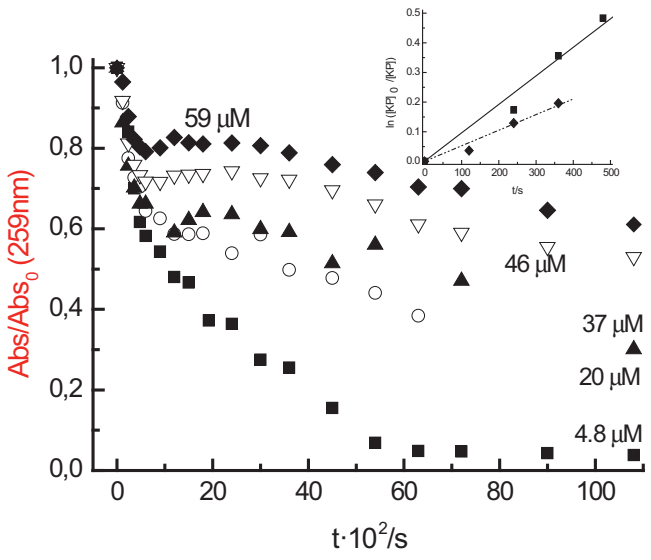

Fig. 3. Pseudo-first order kinetics for the degradation of aqueous **KP** upon irradiation with a medium-pressure Hg lamp at different $[\mathbf{KP}]_0$. [anatase] = 1.0 g L^{-1}, pH ≈ 5.8, $P(O_2) = 21\%$ (v/v), *T ca.* 293 K. Inset: estimation of k_{app}.

Table 2
Apparent first order rate constants found in the photodegradation of aqueous KP. In bold experimental conditions used here as reference. [Anatase] = 1.0 g L^{-1}; [20-MWCNT–TiO_2] = 1.2 g L^{-1} (implies 1.0 g L^{-1} of TiO_2); $pH_{natural}$ c.a. 5.5; *T ca.* 293 K.

Lamp	[KP]/mM	Catalyst	%O_2	[H_2O_2]/mM	pH	$k_{app} \times 10^4/s^{-1}$	$t_{1/2}$/min
UV (254 nm)	59	None	21	0	Natural	3.3 ± 0.4	34.8
	59	None	21	1	Natural	15.8 ± 0.7	7.3
	59	Anatase	21	0	Natural	21.5 ± 0.6	5.3
	59	Anatase	21	3	Natural	16 ± 1	7.2
	59	Anatase	21	30	Natural	12.3 ± 0.5	9.4
	59	20-MWCNT–TiO_2	21	0	Natural	42 ± 3	2.7
UVA–vis (366 nm)	59	None	21	0	Natural	1.33 ± 0.07	86.5
	59	Anatase	21	0	Natural	5.3 ± .0.4	21.7
	4.8	Anatase	21	0	Natural	9.6 ± 0.5	12.0
	20	Anatase	21	0	Natural	9.2 ± 0.5	12.5
	37	Anatase	21	0	Natural	9.2 ± 0.5	12.6
	46	Anatase	21	0	Natural	7.1 ± 0.4	16.2
	59	Anatase	21	0	2.4	1.8 ± 0.2	63.9
	59	Anatase	21	0	11.4	24.2 ± 0.8	4.8
	59	Anatase	50	0	Natural	6.5 ± 0.4	17.7
	59	Anatase	75	0	Natural	6.6 ± 0.6	17.4
	59	Anatase	100	0	Natural	6.9 ± 0.4	16.7
	59	20-MWCNT–TiO_2	21	0	Natural	9.0 ± 0.6	12.8
	59	Anatase	0	0	Natural	12.6 ± 0.9	9.1
	59	Anatase[a]	0	0	Natural	36 ± 3	3.2
	59	Anatase	0	1	Natural	13.0 ± 0.7	8.5
	59	Anatase	0	3	Natural	11.3 ± 0.8	10.2
	59	Anatase	0	6	Natural	8.3 ± 0.2	13.9
	59	20-MWCNT–TiO_2	0	0	Natural	13.6 ± 0.7	8.5
	59	P25	0	0	Natural	1.9 ± 0.2	60.5
	30	20-MWCNT–TiO_2	0	0	Natural	17 ± 2	6.8

[a] [Anatase] = 0.5 g L^{-1}.

between **KP** and the reactive species should increase, but the interpretation needs to take into account the surface phenomena: there are more **KP**, intermediate and photoproducts competing for adsorption onto active sites on the photocatalyst surface, thus leading to an effective reduction in reaction rate [73].

3.2.2. Influence of the acidity of the medium

The photodegradation of aqueous **KP**, under UVA–vis irradiation and air, was carried out at natural pH(=5.2), and also under acid (pH = 2.4) and alkaline (pH = 11.2) conditions. The obtained results are shown in Fig. 4 and the corresponding apparent first order rate constants collected in Table 2.

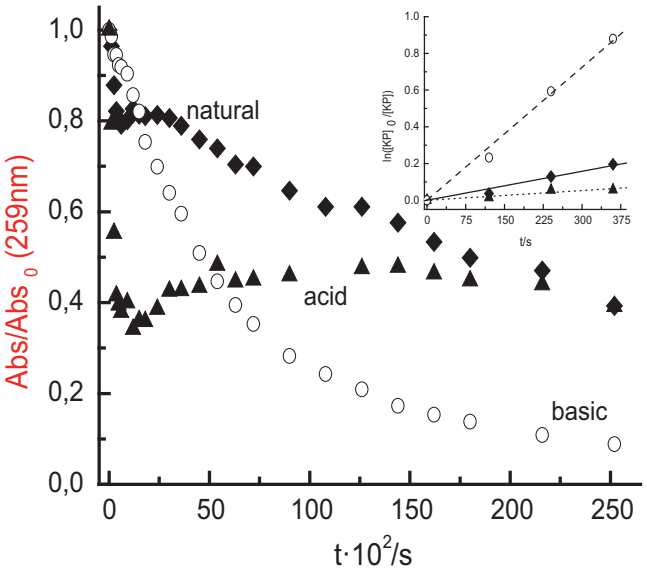

Fig. 4. Influence of the acidity of the medium on the aqueous degradation of **KP** upon irradiation with a medium-pressure Hg lamp. [**KP**] = 59 μM, [anatase] = 1.0 g L^{-1}, $pH_{acid} \approx 2.4$, $pH_{natural} \approx 5.2$, $pH_{basic} \approx 11.4$, P(O_2) = 21% (v/v), *T ca.* 293 K). Inset: estimation of k_{app}.

Usually, the influence of the acidity on heterogeneous photocatalysis processes is complex; it affects the state of protonation of the substrate, and also the charge of phocatalyst (TiO_2) particles (*i.e.*: ionization state of the surface of the catalyst), the size of aggregates (if formed), and the position (energy) of CB and VB and, therefore, E_G [74]. The photocatalyst surface protonates and deprotonates under acidic and alkaline conditions, respectively [74,75,76]:

$$TiOH_2^+ \leftrightarrow TiOH + H^+ \quad pK_{a,TiOH_2+} = 2.4$$

$$TiOH + HO^- \leftrightarrow TiO^- + H_2O \quad pK_{a,TiOH} = 8.0$$

thus, the speciation with pH implies [TiOH] ≥ 80% when 3 < pH < 10, [TiO^-] ≥ 20% if pH > 10; [$TiOH_2^+$] ≥ 20% at pH < 3 [76].

The point of zero charge (PZC) of commercial anatase is 6.00 ± 0.90 [43], *i.e.* its surface will remain positively charged when 2.4 ≤ pH ≤ 5.2, whereas it will be negatively charged at pH = 11.2. The acidity also influences the amount of hydroxyl radicals (HO•) formed by reaction between h^+ and H_2O/HO^-. At neutral or low pH, h^+ are considered the main oxidant species, while at high pH the predominant species is HO• [53].

KP, for which $pK_a = 5.0 \pm 0.2$, shows an unusual pH-dependent photochemistry [14]: the neutral form behaves as a conventional benzophenone with an important intersystem crossing yield to give a triplet excited state, while **KP**$^-$, present at physiological pH, undergoes rapid decarboxylation to **CA**$^-$, which leads to 3-ethylbenzophenone (**1**) as mayor photoproduct (Scheme 2).

The obtained results show the fastest reaction takes place in alkaline medium. High pH values speed the photodegradation, even if the adsorption of **KP**$^-$ onto the negatively charged surface of the photocatalyst is disfavoured. Higher concentration of HO• is produced by the reaction between photogenerated holes and adsorbed OH^-, *i.e.*, $h^+_{VB} + HO^- \rightarrow$ HO•, in alkaline conditions [67].

To prove the participation of HO• in the photocatalyzed degradation of aqueous **KP**, a kinetic run was carried out using commercial

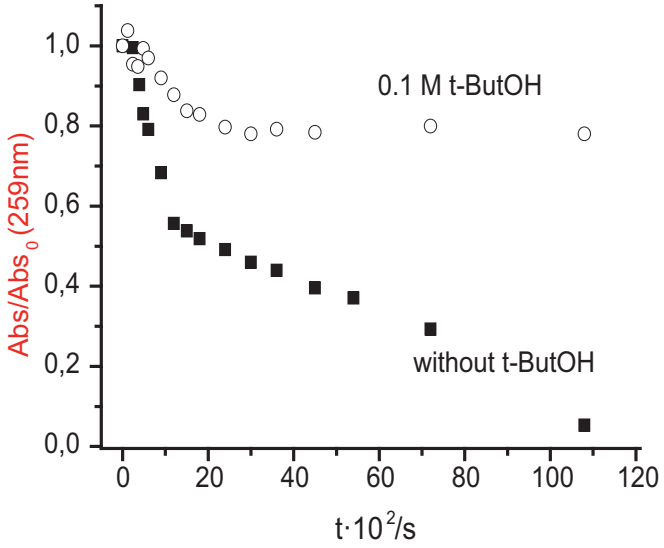

Fig. 5. Pseudo-first order kinetics for the degradation of 59 μM aqueous **KP** upon irradiation with a medium-pressure Hg lamp in the presence and absence of 0.1 M t-ButOH. [commercial anatase] = 1.0 g L^{-1}, pH$_{natural}$ ≈ 5.5, P(O_2) = 21% (v/v), *T ca.* 293 K.

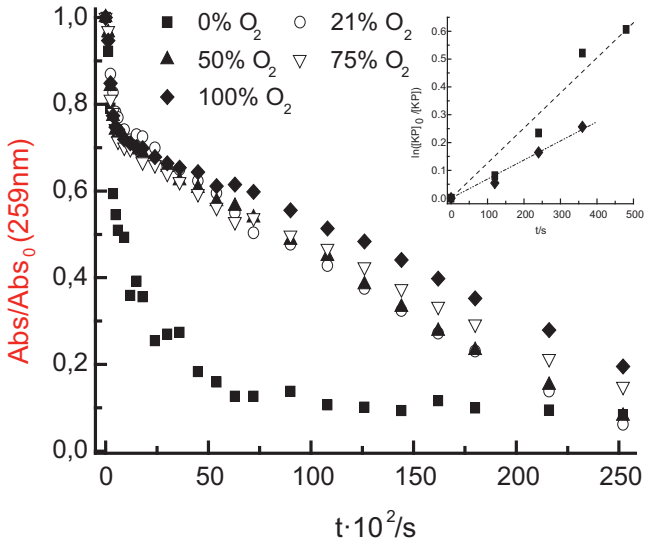

Fig. 6. Effect of O_2 on the photodegradation kinetics of aqueous **KP** upon irradiation with a medium-pressure Hg lamp. Amount of O_2 expressed as percentage in volume. [**KP**] = 59 μM, [anatase] = 1.0 g L^{-1}; *T ca.* 293 K, pH *ca.* 5. Inset: estimation of k_{app}.

anatase under UVA–vis irradiation in the presence of t-BuOH, a known HO• scavenger. The corresponding absorbance *vs*. time profile is shown in Fig. 5.

The presence of t-BuOH slows the photodegradation reaction rate by *ca.* 77%: $k_{app} = (4.4 \pm 0.3) \times 10^{-4}\ s^{-1}$ as compared to $k_{app} = (1.0 \pm 0.1) \times 10^{-4}\ s^{-1}$ when HO• is scavenged. Thus, HO• participation in the process is unequivocally demonstrated, as well as the existence of alternative reaction pathways for **KP** degradation, such as decarboxylation into **1** (Scheme 5).

3.2.3. *Effect of O_2*

The amount of O_2 adsorbed onto the photocatalyst surface depends on the concentration of dissolved O_2, which relates to the partial pressure of oxygen through Henry's law. O_2 partial pressure was controlled by diluting it in Ar before saturating the solution. When oxygen is regularly supplied, the coverage at the surface of titania could be considered constant, and its contribution to the reaction rate can be integrated into the apparent rate constant [74].

The influence of O_2 on the photodegradation of **KP** is shown in Fig. 6, and the correspondingly obtained k_{app} collected in Table 2.

The photodegradation of **KP** is faster in the absence of molecular oxygen. Furthermore, no spectral interferences between **KP** and its photoproducts are observed in time-resolved spectra in anaerobic conditions. The main change takes place between the absence of oxygen and under air-saturation conditions: an increase in O_2 slightly increases the reaction rate, likely the maximum surface coverage by oxygen is reached near the 21% O_2, *i.e.*, air. A similar behavior has been found by Szabo et al. [25].

An increase in the reaction rate could be expected, as oxygen acts as an e^- acceptor, reducing e^-–h^+ recombination, which largely decreases the efficiency of the photocatalytic process. As the photodegradation of **KP** is not only taking place in a pure photocatalytic regime, direct photodegradation also plays its role: the reaction in the presence of O_2 is slower, as it is acting as an efficient triplet state quencher.

KP shows the same absorption spectrum in ethanol and isopentane, and emission spectrum identical to that of benzophenone. In glassy ethanol the phosphorescence spectrum, obtained by excitation of **KP** at 313 nm, exhibits a fingered pattern of vibrational structure with a maximum at 445 nm, which shifts to the red by *ca.* 10 nm when dissolved in isopentane [18]. Thus, in water, more polar than ethanol, a blue shift is expected. The observed **KP** spectrum of fluorescence in water shows its maximum at 343 nm, therefore the **KP** phosphorescence band should lie between 370 and 435 nm, which means that irradiation with UVA–vis lamp (366 nm) is enough to excite **KP**, which crosses to the triplet state with high intersystem crossing yield.

3.2.4. *Photocatalyzed degradation of **KP** under Ar atmosphere*

In the absence of O_2, under UVA–vis irradiation and using 20-MWCNT–TiO_2 as photocatalyst kinetic runs are faster than under air atmosphere, and show the same behavior if [**KP**]$_0$ is varied, *i.e.:* higher k_{app} than synthesized anatase, and the lower [**KP**] the faster the reaction rate (see Table 2).

Standard P25 was used as photocatalyst for comparison purposes. The observed rate constant was $k_{app} = (1.9 \pm 0.2) \times 10^{-4}\ s^{-1}$, *ca.* one order of magnitude lower than that of synthesized anatase, which is the more photoactive crystalline form of TiO_2 [77,78]. In addition to the photoactivity of the allotropic form, other factors, such as impurities, surface and density of hydroxyl groups play a role in the photocatalytic process [79,80].

3.2.5. *Load of photocatalyst*

The optimum load of catalyst is a relevant parameter in practical applications to avoid an excess of catalyst in solution, ensuring optimal photon absorption and reducing light scattering. Anatase concentration was varied between 0.5 and 1.2 g L^{-1}, finding the optimum photocatalyst load at the lower limit, *ca.* 0.5 g L^{-1}, for which $k_{app} = (36 \pm 3) \times 10^{-4}\ s^{-1}$.

Usually, the optimal load of catalyst found in heterogeneous catalysis is attributed to the combination of two opposite factors: a positive one, more catalyst makes available more active sites for adsorption, and a negative one, higher load implies higher light scattering, that reduces the efficiency of photogeneration of e^-/h^+ pairs [81]. Besides, pure photolytic processes are hampered by high concentrations through increased collisional deactivation of excited states [82].

3.2.6. *Effect of H_2O_2*

Fig. 7 shows the effect of H_2O_2 addition on the photodegradation of aqueous **KP** under UVA–vis irradiation. The corresponding kinetic data (k_{app} and $t_{1/2}$) are compiled in Table 2.

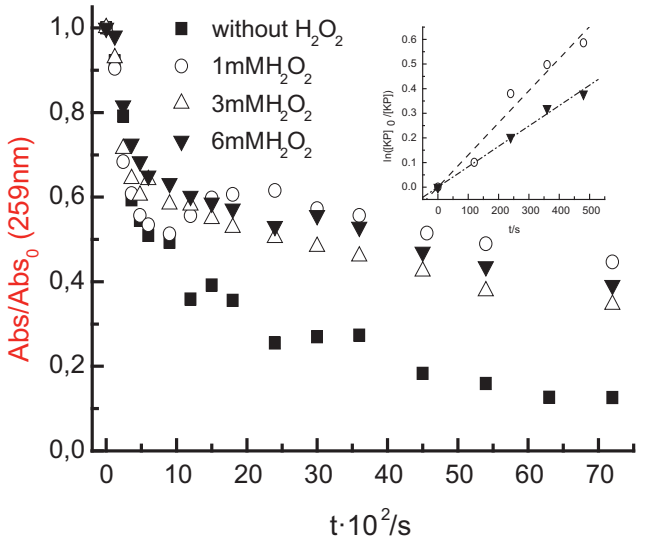

Fig. 7. Pseudo-first order kinetics for the degradation of 59 μM aqueous **KP** upon irradiation with a medium-pressure Hg lamp at different [H_2O_2], [anatase] = 1.0 g L^{-1}; Ar-saturated; *T ca.* 293 K. Inset: estimation of k_{app}.

k_{app} slightly increases with the addition of 1 mM H_2O_2, and decreases at higher concentrations. The quantum yield for the photocatalyzed process decreases due to recombination of the photogenerated e^-/h^+ pairs, which can be prevented by adding a proper electron acceptor to the solution, such as O_2 or inorganic oxidants (H_2O_2, $Na_2S_2O_8$, $KClO_3$, $KBrO_3$, or KIO_4).

The addition of H_2O_2 has two opposite effects: prevention of the recombination of the photogenerated e^-/h^+ pairs, expected to speed up the photocatalyzed degradation, and decrease in the reaction rate as H_2O_2 concentration increases, due to reaction between $HO^\bullet$ and H_2O_2, and to the adsorption of the co-oxidant H_2O_2 onto TiO_2, thus reducing the oxidant capacity of the system [46].

Experiments under UV irradiation were carried out in aerated aqueous solution, using 3 and 30 mM H_2O_2, in the presence of 1.0 g L^{-1} anatase. 1 mM of H_2O_2 was used in the absence of catalyst (pure photolytic regime). The obtained results are shown in Fig. 8. The so-obtained k_{app} and the corresponding half-life times are collected in Table 2.

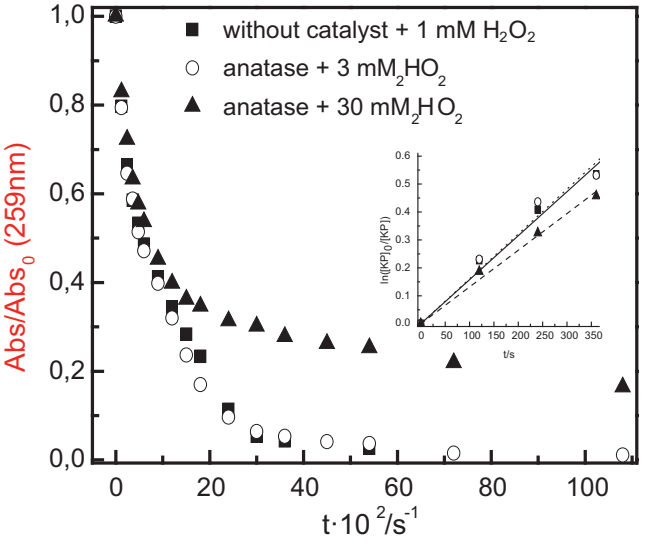

Fig. 8. Kinetic traces obtained for the degradation of aqueous **KP** upon irradiation with a low-pressure Hg lamp at different [H_2O_2]. [anatase] = 1.0 g L^{-1}, pH ≈ 5.3, P(O_2) = 21% (v/v), *T ca.* 293 K. Inset: estimation of k_{app}.

The more efficient degradation takes place either with 1.0 g L^{-1} of anatase and 3 mM H_2O_2, or when aqueous **KP** is photolyzed without catalyst (pure photolytic regime) in presence of H_2O_2 (1 mM). These results and the effect of reduction in k_{app} at higher H_2O_2 concentrations are similar to those found under UVA–vis irradiation.

3.3. Electronic structure calculations

pK_a values and E° (*vs.* NHE) for **KP** and related species are collected in Fig. 9. The value of the pK_a linking **KP** and **KP**$^-$ is *ca.* 1.5 units higher than the experimental one (*ca.* 5). On the other hand, calculations predict, as expected, the negligible presence of the corresponding protonated ketyl species.

The value obtained for the pK_a of the radical anion of **KP** implies its existence and/or that of the corresponding deprotonated form depending on the acidity of the medium. Considering the acid ionization equilibrium of the radical cation, just **KP**$^\bullet$ is predicted to be present, independently of the pH.

The value obtained for E° (**KP**/**KP**$^{\bullet-}$) is similar to that of obtained by Amankwa and Chatten [83] and by Lhiaubet et al. (−1.49 *vs.* NHE) [84] and a bit far from that reported by Michaud et al. (−2.06 V *vs.* NHE) [85].

Gibbs free energies and standard reduction potentials for **KP** and related radical species are collected in Fig. 10. Taking into account the following E° values [86,87]:

$$h^+ + H_2O_{ads} \rightarrow H_2O^{\bullet+} (\rightarrow H^+ + HO^\bullet) \quad E^0 = 2.53 \text{ V}$$

$$H_2O + e^- \rightarrow e^-_{solv} \quad E^0 = -2.87 \text{ V}$$

$$HO^\bullet + e^- \rightarrow HO^- \quad E^0 = 1.90 \text{ V}$$

$$O_2 + e^- \rightarrow O_2^{-\bullet} \quad E^0 = -0.33 \text{ V}$$

and assuming that the E° for **KP** and related species would be similar when adsorbed onto TiO_2, it follows that the oxidation of **KP** and **KP**$^-$ by h^+ and/or $HO^\bullet$, to produce the radical cation **KP**$^{\bullet+}$ and the neutral radical **KP**$^\bullet$, respectively, is feasible. The decarboxylation of the latter is exoergonic, while the rest of the processes are endoergonic: they do not take place upon thermal activation, their barriers being equal or higher than the calculated values. This energy requirement is overcome by photochemical activation.

The pK_a involving the 3-ethylbenzophenone ketyl biradical (^{3}**BCH**) anion has also been calculated:

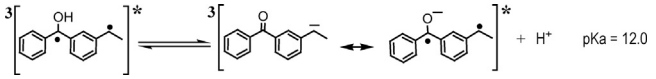

Such pK_a is *ca.* 2 units higher than the experimental value, a *bias* similar to that found for the pK_a of ketoprofen in its ground state (*vide supra*).

4. Total organic carbon

The analysis of the total organic carbon (TOC) provides information about the photoefficiency of the process in terms of the pollution abatement. TOC analysis of aliquots from experiments, under UVA–vis irradiation with 1.2 g L^{-1} 20-MWCNT–TiO_2 at natural pH in the absence and presence of O_2, were carried out at selected times (Fig. 11).

Absence of O_2 improves the efficiency of the photocatalyzed degradation only in the first stages of the process. After 30 min, the mineralization in the absence of O_2 is *ca.* 60%, whereas in air it goes down to *ca.* 43%. This reflects the distinct rate at which the generated intermediates react under different conditions.

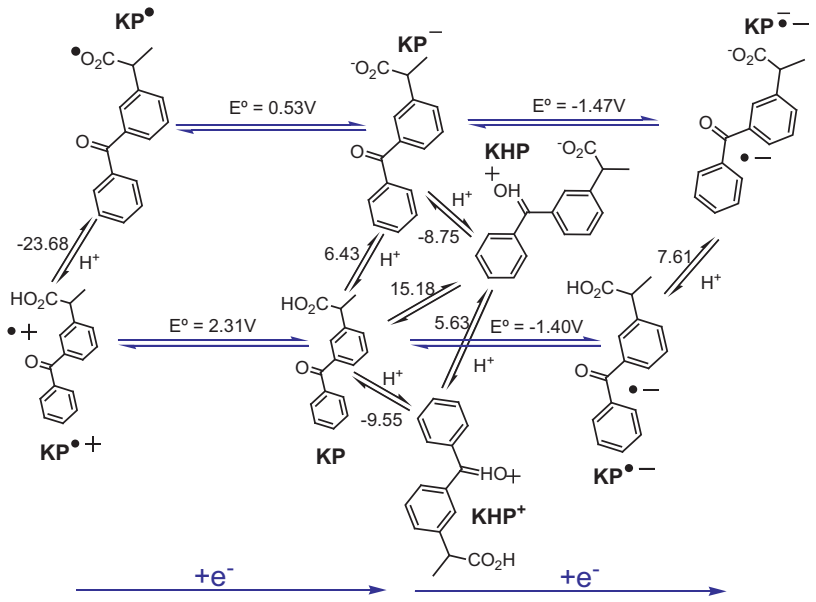

Fig. 9. pK_a values and standard reduction potentials (*vs.* NHE) for **KP** and related radical species in aqueous solution (SMD model) at 298 K. Level of calculation: B3LYP/6-311++G(d,p).

5. Reaction mechanism

Samples were taken at different irradiation times and analyzed for photoproducts, first by HPLC/UV–vis and then by high resolution mass spectrometry (see Section 2). The chromatograms showed a number of peaks, of which only the main ones were selected for identification. The conditions of the experiments are determinant for the nature of the photoproducts (Table 3).

Considering the photoproducts identified by HPLC-MS, and related data found in the literature [19,22,88,89], Scheme 5 shows the proposed mechanism of **KP** aqueous photodegradation through direct photolysis and photocatalysis with TiO_2. Although some m/z ratios may have alternative structural proposals, these would not account for the intermediates and/or photoproducts observed.

In the photodegradation under the pure photolytic regime the decarboxylation of **KP** (t_R 11.92 min, m/z = 255 g/mol) is promoted by light absorption to yield a carbanion (**CA**$^-$)-structurally resonant with 3-ethylbenzophenone ketyl biradical anion (^{3}**BC**$^-$)-which is the precursor of (3-ethylphenyl)(phenyl)methanone **1** (t_R 9.24 min, m/z = 211 g/mol), this is the most relevant among the rest of photoproducts. Although less relevant in direct photolysis, photoproduct **1** could also be the result of a biphotonic process to

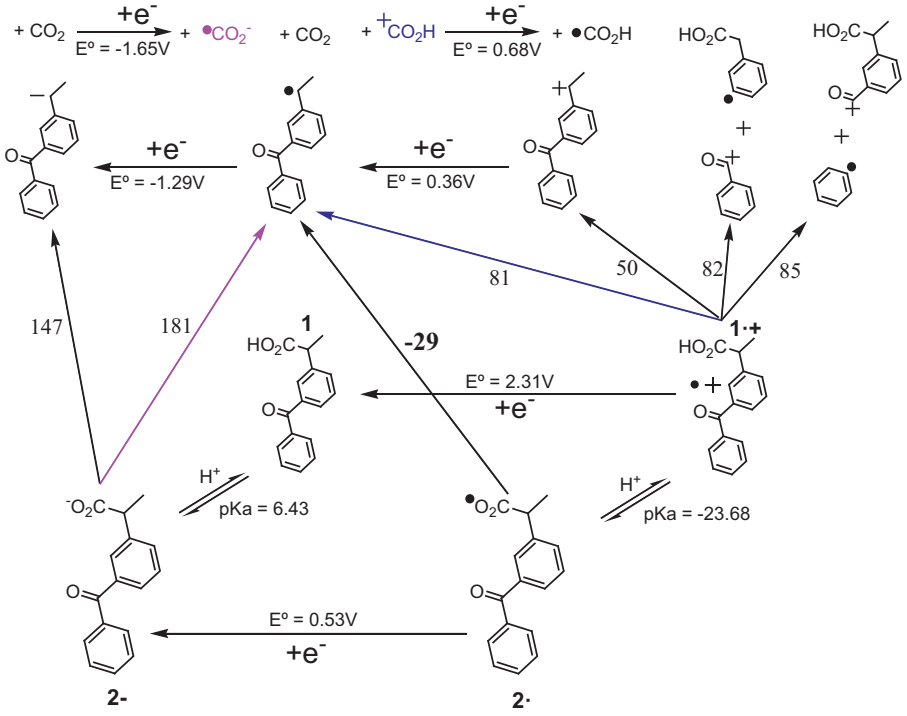

Fig. 10. Thermodynamic values and E° (*vs.* NHE) for **KP** and related radical species in aqueous solution (SMD model) at 298 K. Level of calculation: B3LYP/6-311++G(d,p).

Table 3
Photoproducts (numbered according to Schemes 2 and 5) obtained upon degradation of **KP** after photocatalysis upon UV or UVA–vis irradiation. [KP] = 59 mM; $pH_{natural}$ *ca.* 5.5; *T ca.* 293 K.

Lamp	Catalyst	$\%O_2$	$[H_2O_2]$/mM	pH	Photoproducts
UV (254 nm)	None	21	0	Natural	**1,2,3,4,5,7,8**
	Anatase	21	0	Natural	**1,2,3,4,6,7,8,9,10**
	Anatase	21	3	Natural	**3,4,8,10**
	20-MWCNT–TiO_2	21	0	Natural	**1,3,4,6,10**
UVA–vis (366 nm)	None	21	0	Natural	**1,2,3,4,5,6,10**
	Anatase	21	0	Natural	**1,2,3,4,5,6,10**
	Anatase	21	0	2.4	**2,3,4,6,10**
	Anatase	21	0	11.4	**4,5,6,8,10**
	Anatase	0	0	Natural	**1,2,3,4,5,9,10**
	20-MWCNT–TiO_2	0	0	Natural	**1,2**

generate **KP•** from **KP**$^-$, its decarboxylation and further addition of **H•** to **BC•**. This intermediate could also be formed from ^{3}**BC**$^-$.

The ketyl radical **BC•** could lead to **3** (t_R 10.33 min, m/z = 227 g/mol) after HO• addition or by other pathway produce photoproduct **2** (t_R 9.66 min, m/z = 209 g/mol) by elimination of H•. Further reduction of **2**, through elimination of oxygen, yields **5** (t_R 12.51 min, m/z = 195 g/mol).

Further hydroxylation by **HO•** produces many hydroxylation products (**12**) [27] and dimerization products like **11** are also possible.

Oxidation of photoproduct **3** would lead to product **4** (t_R 10.81 min, m/z = 225 g/mol) from which benzophenone **6** (t_R 10.35 min, m/z = 181 g/mol) could be generated by elimination of the acetaldehyde group. Also from **4** acetophenone **9** (t_R 9.69 min, m/z = 121 g/mol) could be formed. Both photoproducts **6** and **9** could be precursors of the epoxide **10** (t_R 10.34 min, m/z = 105 g/mol). The formation of photoproduct **7** (t_R 8.87 min, m/z = 243 g/mol) could be the result of the reaction between the hydroxyl radical and **BC•**, and subsequent addition of H•.

In addition to the described processes this compound could suffer other radical reactions and homolytic/heterolytic bond breakages at sites other than the lateral chain, which could explain the formation of photoproduct **8** (t_R 11.32 min, m/z = 195 g/mol). In addition to the described photoproducts, Szabo et al. have also found small and stable carboxylic acids (propionic, acetic, oxalic, *etc.*) [25]

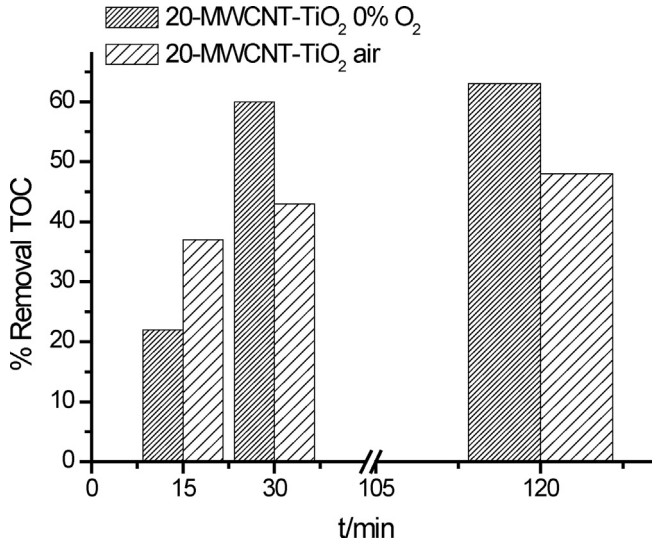

Fig. 11. Total organic carbon analysis for the photocatalyzed degradation of aqueous **KP** under UVA–vis irradiation. $[KP]_0$ = 59 mM, [20-MWCNT–TiO_2] = 1.2 g L^{-1}; $pH_{natural}$ *ca.* 5.5, *T ca.* 293 K.

On the other hand, the photocatalytic pathway involves the adsorption of the neutral and anion forms of **KP** onto TiO_2 surface, which after light irradiation generates surface bound electrons and positive holes, the latter being the source of hydroxyl radicals. Both h^+ and HO• could react with ketoprofen carboxylate (**KP**$^-$) to yield the intermediate **KP•**, which after decarboxylation produces the ketyl radical **BC•**$^-$; then this intermediate reacts as described in the direct photolytic pathway, thus the final photoproducts are the same in both cases. The neutral form could also react with h^+ and/or HO• to give the corresponding radical cation (**KP•**$^+$) which could decarboxylate to the ketyl radical **BC•** or suffer homolytic/heterolytic bond cleavages to end up in photoproducts like **2**, **8** and **10**. Finally neutral ketoprofen (**KP**) could react with e^- to generate the corresponding radical anion (**KP•**$^-$), which reacts in the same way as in the case of the pure photolytic regime.

6. Conclusions

Under UV irradiation **KP** photodegradation in natural pH takes place faster with 1.2 g L^{-1} of synthesized 20-MWCNT–TiO_2 as catalyst and $P(O_2)$ = 21% (v/v) at *ca.* 293 K, the half-life time being 165 s. Complete removal of **KP** is achieved.

Under UVA–vis irradiation the best catalyst is also 20-MWCNT–TiO_2 both in the presence and absence of O_2, the photodegradation is at least 1.4 times faster than with synthesized anatase in the same conditions ([anatase] = 1 g L^{-1}, $P(O_2)$ = 21% (v/v) at *ca.* 293 K. In aerobic conditions there is no influence of the content of dissolved O_2, and the reaction is *ca.* 4 times faster in basic media than in natural pH. The photodegradation of **KP** by P25 is six times slower than with anatase and almost an order of magnitude than with 20-MWCNT–TiO_2.

Ten photoproducts have been identified, the main being (3-ethylphenyl)(phenyl)methanone (**1**) with m/z = 211 g/mol, both in aerobic and anaerobic conditions. Similar photoproducts have been found under both the pure photolytic regime and by photocatalysis.

Gibbs free energies, pK_a values and standard reduction potentials for **KP** and related radical species in aqueous solution (SMD model) were calculated by DFT (B3LYP/6-311 G(d,p)). The results agree with the experimental behavior.

The proposed mechanism includes the photodegradation of **KP** in aqueous solution under the pure photolytic regime and by photocatalysis. In both cases similar intermediates play a role which explains the formation of same photoproducts, faster with photocatalysts under the same irradiating conditions.

Acknowledgements

This work was funded by the Xunta de Galicia (Spain) through Project PGIDIT05TAM10301PR and the INCITE07PXI103184ES action and the Ministerio de Ciencia e Innovación through project ACI2010-1093. CM also thanks the UDC for funding a research stay

at the Universidade do Porto. Authors wish to thank Centro de Supercomputación de Galicia (CESGA) for computing facilities.

References

[1] V.J.W. Pereira, H.S. Linden, K.G.P.C. Singer, Environmental Science and Technology 41 (2007) 1682–1688.
[2] J.L. Santos, I. Aparicio, M. Callejón, E. Alonso, Journal of Hazardous Materials 164 (2009) 1509–1516.
[3] S. González Alonso, M. Catalá, R.R. Maroto, J.L.R. Gil, Á.G. de Miguel, Y. Valcárcel, Environment International 36 (2010) 195–201.
[4] K. Fent, A.A. Weston, D. Caminada, Aquatic Toxicology 76 (2006) 122–159.
[5] C.G. Daughton, T.A. Ternes, Environmental Health Perspectives 107 (1999) 907–938.
[6] C. Férnandez, M. González-Doncel, J. Pro, G. Carbonell, J.V. Tarazona, Science of the Total Environment 408 (2010) 543–551.
[7] E. Gracia-Lor, J.V. Sancho, R. Serrano, F. Hernandez, Chemosphere 87 (2012) 453–462.
[8] K.A.K. Musa, J.M. Matxain, L.A. Eriksson, Journal of Medicinal Chemistry 50 (2007) 1735–1743.
[9] T. Suzuki, Y. Osanai, T. Isozaki, Photochemistry and Photobiology 88 (2012) 884–888.
[10] Y. Tokura, Journal of Dermatological Science 23 (2000) S6–S9.
[11] C. Foti, N. Cassano, G.A. Vena, G. Angelini, Contact Dermatitis 64 (2011) 181–183.
[12] M. Lukeman, J.C. Scaiano, Journal of the American Chemical Society 127 (2005) 7698–7699.
[13] L.J. Martínez, J.C. Scaiano, Journal of American Chemical Society 119 (1997) 11066–11070.
[14] G. Cosa, Martinez, J. Lydia, J.C. Sacaiano, Physical Chemistry Chemical Physics 1 (1999) 3533–3537.
[15] S. Monti, S. Sortino, G. De Guidi, G. Marconi, Journal of Chemical Society, Faraday Transactions 93 (1997) 2269–2275.
[16] S. Monti, S. Sortino, G. De Guidi, G. Marconi, New Journal of Chemistry (1998) 599–604.
[17] C.D. Borsarelli, S.E. Braslavsky, S. Sortino, G. Marconi, S. Monti, Photochemistry and Photobiology 72 (2000) 163–171.
[18] V. Lhiaubet, F. Gutierrez, F. Penaud-Berruyer, E. Amouyal, J.-P. Daudey, R. Poteau, N. Chouini-Lalanne, N. Paillous, New Journal of Chemistry 24 (2000) 403–410.
[19] F. Bosca, M.A. Miranda, G. Carganico, D. Mauleon, Photochemistry and Photobiology 60 (1994) 96–101.
[20] L.L. Costanzo, G. De Guidi, G. Condorelli, A. Cambria, M. Fama, Photochemistry and Photobiology 50 (1989) 359–365.
[21] G. Cosa, M. Lukeman, J.C. Scaiano, Accounts of Chemical Research 42 (2009) 599–607.
[22] V. Matamoros, A. Duhec, J. Albaiges, J.M. Bayona, Water Air and Soil Pollution 196 (2009) 161–168.
[23] T. Kosjek, S. Perko, E. Heath, B. Kralj, D. Zigon, Journal of Mass Spectrometry 46 (2011) 391–401.
[24] S. Mas, R. Tauler, A. de Juan, Journal of Chromatography A 1218 (2011) 9260–9268.
[25] R.K. Szabo, C. Megyeri, E. Illes, K. Gajda-Schrantz, P. Mazellier, A. Dombi, Chemosphere 84 (2011) 1658–1663.
[26] A. Kimura, M. Osawa, M. Taguchi, Radiation Physics and Chemistry 81 (2012) 1508–1512.
[27] M.A. Oturan, J. Pinson, J. Bizot, D. Deprez, B. Terlain, Journal of Electroanalytical Chemistry 334 (1992) 103–109.
[28] E. Illes, E. Takacs, A. Dombi, K. Gajda-Schrantz, K. Gonter, L. Wojnarovits, Radiation Physics and Chemistry 81 (2012) 1479–1483.
[29] G.E. Adams, R.L. Willson, Journal of the Chemical Society-Faraday Transactions I 69 (1973) 719–729.
[30] E. Hayon, M. Simic, T. Ibata, N.N. Lichtin, Journal of Physical Chemistry 76 (1972) 2072–2078.
[31] Y.C. Xu, X.B. Chen, W.H. Fang, D.L. Phillips, Organic Letters 13 (2011) 5472–5475.
[32] M.D. Li, C.S. Yeung, X.G. Guan, J.N. Ma, W. Li, C.S. Ma, D.L. Phillips, Chemistry-A European Journal 17 (2011) 10935–10950.
[33] Y.P. Chuang, J.D. Xue, Y. Du, M.D. Li, H.Y. An, D.L. Phillips, Journal of Physical Chemistry B 113 (2009) 10530–10539.
[34] M.D. Li, J.N. Ma, T. Su, M.Y. Liu, L.H. Yu, D.L. Phillips, Journal of Physical Chemistry B 116 (2012) 5882–5887.
[35] O. Legrini, E. Oliveros, A.M. Braun, Chemical Reviews 93 (1993) 671–698.
[36] M. Klavarioti, D. Mantzavinos, D. Kassinos, Environment International 35 (2009) 402–417.
[37] Y.X. Jin, G.H. Li, Y. Zhang, Y.X. Zhang, L.D. Zhang, Journal of Physics-Condensed Matter 13 (2001) L913–L918.
[38] T.E. Doll, F.H. Frimmel, Water Research 38 (2004) 955–964.
[39] T.E. Doll, F.H. Frimmel, Water Research 39 (2005) 403–411.
[40] T.E. Doll, F.H. Frimmel, Catalysis Today 101 (2005) 195–202.
[41] M. Canle, M.I. Fernandez, S. Rodriguez, J.A. Santaballa, S. Steenken, E. Vulliet, ChemPhysChem 6 (2005) 2064–2074.
[42] E. Beetge, J. du Plessis, D.G. Müller, C. Goosen, F.J. van Rensburg, International Journal of Pharmaceutics 193 (2000) 261–264.
[43] M.L. Canle, J.A. Santaballa, E. Vulliet, Journal of Photochemistry and Photobiology A: Chemistry 175 (2005) 192–200.
[44] W.D. Wang, C.G. Silva, J.L. Faria, Applied Catalysis B-Environmental 70 (2007) 470–478.
[45] W. Wang, P. Serp, P. Kalck, J.L. Faria, Journal of Molecular Catalysis A: Chemical 235 (2005) 194–199.
[46] C. Martínez, M.L. Canle, M.I. Fernández, J.A. Santaballa, J. Faria, Applied Catalysis B: Environmental 102 (2011) 563–571.
[47] H.J. Kuhn, S.E. Braslavsky, R. Schmidt, Pure and Applied Chemistry 76 (2004) 2105–2146.
[48] J.A. Santaballa, H. Maskill, M.C. López, Investigating Organic Reaction Mechanisms, Blackwell Publishing Ltd., Oxford, 2006.
[49] G.W.T.M.J. Frisch, H.B. Schlegel, G.E. Scuseria, M.A. Robb, J.R. Cheeseman, J.A. Montgomery, T. Vreven Jr., K.N. Kudin, J.C. Burant, J.M. Millam, S.S. Iyengar, J. Tomasi, V. Barone, B. Mennucci, M. Cossi, G. Scalmani, N. Rega, G.A. Petersson, H. Nakatsuji, M. Hada, M. Ehara, K. Toyota, R. Fukuda, J. Hasegawa, M. Ishida, T. Nakajima, Y. Honda, O. Kitao, H. Nakai, M. Klene, X. Li, J.E. Knox, H.P. Hratchian, J.B. Cross, V. Bakken, C. Adamo, J. Jaramillo, R. Gomperts, R.E. Stratmann, O. Yazyev, A.J. Austin, R. Cammi, C. Pomelli, J.W. Ochterski, P.Y. Ayala, K. Morokuma, G.A. Voth, P. Salvador, J.J. Dannenberg, V.G. Zakrzewski, S. Dapprich, A.D. Daniels, M.C. Strain, O. Farkas, D.K. Malick, A.D. Rabuck, K. Raghavachari, J.B. Foresman, J.V. Ortiz, Q. Cui, A.G. Baboul, S. Clifford, J. Cioslowski, B.B. Stefanov, G. Liu, A. Liashenko, P. Piskorz, I. Komaromi, R.L. Martin, D.J. Fox, T. Keith, M.A. Al-Laham, C.Y. Peng, A. Nanayakkara, M. Challacombe, P.M.W. Gill, B. Johnson, W. Chen, M.W. Wong, C. Gonzalez, J.A. Pople, Gaussian 03, Wallingford CT, 2004.
[50] D.M. Camaioni, C.A. Schwerdtfeger, Journal of Physical Chemistry A 109 (2005) 10795–10797.
[51] A.V. Marenich, C.J. Cramer, D.G. Truhlar, Journal of Physical Chemistry B 113 (2009) 6378–6396.
[52] K.J. Laidler, Pure and Applied Chemistry 68 (1996) 149–192.
[53] Y. Lin, C. Ferronato, N. Deng, F. Wu, J.-M. Chovelon, Applied Catalysis B: Environmental 88 (2009) 32–41.
[54] M.L. Canle, H. Maskill, J.A. Santaballa, Experimental Methods for Investigating Kinetics, Blackwell Publishing Ltd., Oxford, 2007.
[55] N. Serpone, Journal of Photochemistry and Photobiology A: Chemistry 104 (1997) 1–12.
[56] N. Serpone, R. Terzian, D. Lawless, P. Kennepohl, G. Sauvé, Journal of Photochemistry and Photobiology A: Chemistry 73 (1993) 11–16.
[57] N. Serpone, A. Salinaro, Pure and Applied Chemistry 71 (1999) 303–320.
[58] C.C. Wong, W. Chu, Chemosphere 50 (2003) 981–987.
[59] W. Chu, C.T. Jafvert, C.A. Diehl, K. Marley, R.A. Larson, Environmental Science and Technology 32 (1998) 1989–1993.
[60] W. Chu, C.T. Jafvert, Environmental Science and Technology 28 (1994) 2415–2422.
[61] N. Serpone, A.V. Emeline, International Journal of Photoenergy 4 (2002) 91–131.
[62] S.E. Braslavsky, Pure and Applied Chemistry 79 (2007) 293–465.
[63] J.M. Herrmann, Topics in Catalysis 34 (2005) 49–65.
[64] J. Li, P.S.a.J.L. Figueiredo (Eds.), Carbon Materials for Catalysis, Wiley, New Jersey, 2009, pp. 507–533.
[65] N. Daneshvar, A. Aleboyeh, A.R. Khataee, Chemosphere 59 (2005) 761–767.
[66] J.R. Bolton, K.G. Bircher, W. Tumas, C.A. Tolman, Pure and Applied Chemistry 73 (2001) 627–637.
[67] D.G. Crosby, G.R. Helz, R.G. Zepp, Aquatic and Surface Photochemistry, Lewis Publishers, Boca Raton, 1994.
[68] S.-H. Kim, H.H. Ngom, H.K. Shon, S. Vigneswaran, Separation and Purification Technology 58 (2008) 335–342.
[69] J.L. Faria, W. Wang, Carbon Materials in Photocatalysis, John Wiley & Sons, New Jersey, 2009.
[70] K. Woan, G. Pyrgiotakis, W. Sigmund, Advanced Materials 21 (2009) 2233–2239.
[71] M.R. Hoffmann, S.T. Martin, W.Y. Choi, D.W. Bahnemann, Chemical Reviews 95 (1995) 69–96.
[72] Pyrgiotakis Georgios, S.-H. Lee, W. Sigmund, Presented at MRS Spring Meeting, San Francisco, 2005.
[73] G. Marci, V. Augugliaro, A.B. Prevot, C. Baiocchi, E. Garcia-Lopez, V. Loddo, L. Palmisano, E. Pramauro, M. Schiavello, Annales de Chimie 93 (2003) 639–648.
[74] S. Malato, P. Fernández-Ibáñez, M.I. Maldonado, J. Blanco, W. Gernjak, Catalysis Today 147 (2009) 1–59.
[75] M.M. Haque, M. Muneer, Journal of Hazardous Materials 145 (2007) 51–57.
[76] C. Kormann, D.W. Bahnemann, M.R. Hoffmann, Environmental Science and Technology 25 (1991) 494.
[77] K. Tanaka, M.F.V. Capule, T. Hisanaga, Chemical Physics Letters 187 (1991) 73–76.
[78] C. Martinez, M. Canle, M.I. Fernandez, J.A. Santaballa, J. Faria, Applied Catalysis B-Environmental 107 (2011) 110–118.
[79] H. Tada, M. Tanaka, Langmuir 13 (1997) 360–364.
[80] Z. Ding, G.Q. Lu, P.F. Greenfield, The Journal of Physical Chemistry B 104 (2000) 4815–4820.
[81] B. Neppolian, H.C. Choi, S. Sakthivel, B. Arabindoo, V. Murugesan, Journal of Hazardous Materials 89 (2002) 303–317.
[82] N.J. Turro, V. Ramamurthy, J.C. Scaiano, Principles of Molecupar Photchemistry. An Introduction, University Science Books, Sausalito, CA, 2009.
[83] L. Amankwa, L.G. Chatten, Analyst 109 (1984) 57–60.

[84] V. Lhiaubet, N. Paillous, N. Chouini-Lalanne, Photochemistry and Photobiology 74 (2001) 670–678.
[85] S. Michaud, V. Hajj, L. Latapie, A. Noirot, V. Sartor, P.L. Fabre, N. Chouini-Lalanne, Journal of Photochemistry and Photobiology B-Biology 110 (2012) 34–42.
[86] A. Fujishima, T. Rao, D. Tryk, Journal of Photochemistry and Photobiology C: Photochemistry Reviews 1 (2000) 1–21.
[87] P. Wardman, Journal of Physical and Chemical Reference Data 18 (1989) 1637–1755.
[88] F. Bosca, M.A. Miranda, Journal of Photochemistry and Photobiology B-Biology 43 (1998) 1–26.
[89] P. Pietta, E. Manera, P. Ceva, Journal of Chromatography 390 (1987) 454–457.